ORIGINAL RESEARCH

Y. Nakata
N. Sato
T. Masumoto
H. Mori
H. Akai
H. Nobusawa
Y. Adachi
H. Oba
K. Ohtomo

Parasellar T2 Dark Sign on MR Imaging in Patients with Lymphocytic Hypophysitis

BACKGROUND AND PURPOSE: MR imaging findings of LYH and pituitary adenomas are similar, but the therapeutic strategies are completely different. The purpose of this study was to evaluate sellar and parasellar MR imaging findings in patients with both diseases, as well as characteristic clinical findings.

MATERIALS AND METHODS: Clinical findings, including endocrinologic study and MR images of 20 patients with LYH and 22 patients with pituitary adenoma, were retrospectively reviewed. We evaluated the MR images in relation to the following: 1) the PPHI on T1-weighted images, 2) thickened stalk (>3.5 mm), 3) pituitary symmetry, 4) pituitary enhancement pattern, 5) a dural tail, and 6) parasellar signal intensity on T2- and T1-weighted images.

RESULTS: Between patients with LYH and those with pituitary adenoma, a significant difference was identified for the number of patients with loss of PPHI, thickened stalk, pituitary symmetry, homogeneous enhancement, and parasellar dark signal intensity on T2-weighted images by statistical analysis (Fisher exact probability test, $P < .05$). Among them, only parasellar dark signal intensity on T2-weighted images had no false-positive cases.

CONCLUSIONS: The parasellar T2 dark sign can be a specific finding used to distinguish pituitary adenoma from LYH.

ABBREVIATIONS: ACTH = adrenocorticotrophic hormone; AL = anterior lobe; DI = diabetes insipidus; Dp = desmopressin; FSH = follicle-stimulating hormone; Gc = glucocorticoid; GH = growth hormone; GHs = GH-secreting; ICA = internal carotid artery; IgG4 = immunoglobulin 4; Iso = isointense; L = left; LH = luteinizing hormone; Lt = levothyroxine; LYH = lymphocytic hypophysitis; MRI = MR imaging; Non-f = nonfunctioning; PA = pituitary adenoma; Pan-hypo = panhypopituitarism; Partial-hyper = partial hyperpituitarism; Partial-hypo = partial hypopituitarism; PL = posterior lobe; PPHI = posterior pituitary T1 high intensity; PRL = prolactin; PRLs = PRL-secreting; R = right; synd = syndrome; T1WI = T1-weighted imaging; T2WI = T2-weighted imaging; Ts = testosterone; TSH = thyroid-stimulating hormone

LYH is a rare inflammatory disease of the pituitary gland. This condition is characterized by lymphocytic infiltration and eventual destruction of the pituitary tissue accompanied by various degrees of pituitary dysfunction. This disease is now known to affect both pituitary lobes, at all ages and in both sexes.[1-6] An autoimmune pathogenesis is suggested by several histopathologic, laboratory, and clinical findings.[7]

LYH is often misdiagnosed because its clinical and radiologic features mimic tumors in the sellar and parasellar region.[1] The main diagnostic issue is that LYH is a relatively rare disease, and its imaging findings are not well-recognized in contrast to those of overwhelmingly more common pituitary tumors, pituitary adenomas.[8] Distinguishing LYH from pituitary adenomas is very important because different therapeutic strategies are used to treat the 2 diseases. The treatment of LYH remains controversial, though conservative management with close clinical observation has been advocated on the basis of its often benign transient course.[9,10] The correct diagnosis of LYH contributes to avoiding needless surgery, which is invasive and sometimes results in endocrine dysfunction. However, distinguishing LYH from pituitary adenomas can be difficult. Leung et al[9] reported that even with MR imaging studies, approximately 40% of the cases are misdiagnosed preoperatively as pituitary adenomas. MR imaging findings in patients with LYH and pituitary adenoma were reported in some recent articles.[2,3,8,11-14] However, most previous reports of MR imaging findings of LYH were case reports and/or reviews of the literature.

Recently, we experienced some cases of LYH, which showed dark-signal-intensity areas on T2-weighted images around the pituitary gland and in the cavernous sinus. To the best of our knowledge, no studies have reported such signal-intensity abnormalities. We hypothesized that dark-signal-intensity areas on T2-weighted images around the pituitary gland and in the cavernous sinus were characteristic in patients with LYH and were useful for distinguishing pituitary adenoma from LYH.

The present study was retrospectively performed to review a series of clinical and MR imaging findings in patients with LYH, including signal intensity around the pituitary gland. As

Received March 9, 2010; accepted after revision May 10.

From the Department of Radiology (Y.N., N.S.), National Center Hospital of Neurology and Psychiatry, Tokyo, Japan; Department of Radiology (Y.N., H.M., H.A., K.O.), Faculty of Medicine, University of Tokyo, Tokyo, Japan; Department of Diagnostic Radiology (N.S.), Faculty of Medicine, University of Gumma, Maebashi, Japan; Department of Radiology (T.M.), Faculty of Medicine, University of Tsukuba, Tsukuba, Japan; Department of Radiology (H.N.), Faculty of Medicine, Showa University, Tokyo, Japan; Department of Radiology (Y.A.), University of California, San Francisco, San Francisco, California; Department of Radiology (Y.A., H.O.), Faculty of Medicine, Teikyo University, Tokyo, Japan; and Department of Radiology (H.O.), Showa General Hospital, Tokyo, Japan.

Please address correspondence to Noriko Sato, MD, PhD, Department of Radiology, National Center Hospital of Neurology and Psychiatry, 4-1-1 Ogawahigashi, Kodaira, Tokyo 187-8511, Japan; e-mail address: snoriko@ncnp.go.jp

indicates article with supplemental on-line tables.

DOI 10.3174/ajnr.A2201

a control study, we also evaluated clinical and MR imaging findings in patients with pituitary adenoma for comparison.

Materials and Methods

Patients

We retrospectively reviewed the MR imaging findings in 20 patients with LYH who were selected by review of clinical records. Our local ethics committee did not require its approval or informed consent for this retrospective review. A retrospective review of clinical records in 6 hospitals from 1987 to 2009 revealed 24 patients who were clinically diagnosed as LYH. Two patients who had a history of sarcoidosis or pachymeningitis, and 2 patients whose initial MR images had not been available were excluded from the study. As a consequence, 20 patients with LYH were enrolled. Ten were males and 10 were females, from 9 to 72 years of age, with a mean age of 46.0 ± 19.5 years (On-line Table 1). Four of 20 patients had histologically proved disease by transsphenoidal biopsy. The remaining 16 patients were diagnosed on the basis of clinical and endocrinologic studies, MR imaging findings, response to steroid therapy, and natural clinical course.[4,7] Five patients had a history of autoimmune diseases, such as IgG4-related disorders, rheumatoid arthritis, and bullous pemphigoid. One patient was pregnant.

We also reviewed the clinical and MR imaging findings in 22 patients with pituitary adenoma. A retrospective review of clinical records in 1 hospital from 2002 to 2009 revealed 52 patients who were treated with transsphenoidal resection and had a proved pathologic diagnosis of pituitary adenoma. Sixteen patients who had recurrent pituitary adenomas and underwent a second operation, 11 patients whose pathologies did not differentiate between functioning and nonfunctioning adenoma because immunostaining was not performed, 2 patients whose initial MR images had not been available, and 1 patient who received irradiation due to malignancy were excluded from the study. As a consequence, 22 patients with pituitary adenoma were enrolled. Ten were men and 12 were women, and they ranged in age from 25 to 73 years, with a mean age of 50.3 ± 15.8 years (On-line Table 2). All patients were treated with transsphenoidal resection, and their pathologies were proved.

In all patients with LYH and pituitary adenoma, the plasma concentrations of ACTH, GH, PRL, LH, FSH, TSH, cortisol, free T4, and testosterone were measured. Provocative tests were performed as follows: for TSH and PRL, after a bolus injection of 500 mg of TSH-releasing hormone; for LH and FSH, 100 mg of gonadotropin-releasing hormone; for GH, 100 mg of GH-releasing hormone or 0.1 U of regular insulin per kilogram of body weight; and for cortisol, 0.25 mg of ACTH or 0.1 U of regular insulin per kilogram of body weight. Multiple blood samples were collected to measure plasma hormone concentrations before and for up to 120 minutes after the injections. In patients with LYH except for cases 2, 8, and 13, plasma vasopressin concentrations were determined by radioimmunoassay, and plasma and urinary osmolarities were measured before and after 4–8 hours of water deprivation. In cases 9, 11, 21, and 22 of patients with pituitary adenoma, hormonal examination was done for the posterior lobe by using the same method.

MR Imaging Acquisition

All patients with LYH and pituitary adenoma underwent MR imaging of the sella turcica with 1.5T superconductive units. Patients with LYH underwent MR imaging with 6 units in 6 hospitals, and patients with pituitary adenoma underwent 1 MR imaging in 1 hospital. T1-weighted images were acquired in the coronal and sagittal planes with the following parameters: TR/TE/NEX = 300–660/7.9–23 ms/3–4, a 192 × 256 to 512 × 512 matrix, a 14- to 20-cm FOV, a 3-mm section thickness, and a 0.0- to 0.6-mm intersection gap. T2-weighted sagittal or coronal images were obtained with the following parameters: TR/TE/NEX = 2000–3500/80–120 ms/3–4, a 192 × 256 to 512 × 512 matrix, a 14- to 20-cm FOV, a 3-mm section thickness, and a 0.0- to 0.6-mm intersection gap. T1-weighted images after an intravenous injection of contrast medium (0.1 mmol/kg of body weight) were also acquired, except for case 8, in patients with LYH, in the coronal and sagittal planes with the same parameters as those of the T1-weighted images. All patients with LYH had 1–6 follow-up MR imaging studies performed during a period ranging from 1 month to 8 years.

Two neuroradiologists (Y.N., N.S.) who did not know the patients' clinical information evaluated the MR imaging findings of the patients with LYH and pituitary adenoma. In several recent articles, some findings were reported to be useful for distinguishing pituitary adenoma from LYH, such as precontrast homogeneous signal intensity, intact sellar floor, suprasellar extension, loss of PPHI, stalk thickening, mass symmetry, homogeneous enhancement, and adjacent dural enhancement (the so-called dural tail).[2,3,8,11-14] In this study, evaluation of the precontrast signal intensity was excluded because pituitary adenomas often show complicated signal intensities due to hemorrhagic or cystic changes, and it is a not suitable factor for making a simple assessment. The findings of destruction of the sellar floor and extension to the sphenoid sinus were also excluded because it was obvious that these findings indicate neoplasm. The finding of suprasellar extension was also excluded because it depends on the size of pituitary lesions, and pituitary adenomas vary in size from microadenoma to macroadenoma.

We, therefore, selected the following MR findings as assessment factors: 1) PPHI on T1-weighted images, 2) thickened stalk, 3) pituitary symmetry, 4) pituitary enhancement pattern, 5) the dural tail, and 6) parasellar signal intensity on T2- and T1-weighted images. PPHI was classified as either "identified" or "not identified."[15] If the diameter of the pituitary stalk exceeded 3.5 mm at the level of the median eminence of the hypothalamus, the stalk was considered "thick."[16] Pituitary symmetry was classified as either "symmetric" or "asymmetric."[15] The enhancement pattern was classified as either "homogeneous" or "heterogeneous." The dural tail was classified as either "identified" or "not identified." Parasellar signal intensity on T2- and T1-weighted images was classified as either "dark," "low," "iso," or "high" intensity. On T2-weighted images, "dark" was isointense with bone cortex; "low" was isointense with white matter; "iso" was isointense with gray matter, and "high" was hyperintense with gray matter. On T1-weighted images, "dark" was isointense with bone cortex; "low" was isointense with CSF, "iso" was isointense with gray matter, and "high" was hyperintense with gray matter.[12,17] If different signal intensities were detected in the parasellar areas, the lowest signal intensity was adopted. When the 2 neuroradiologists found different results, they discussed the case and came to a decision by consensus. We also reviewed all images of a series of follow-up MR images in patients who showed parasellar dark-signal-intensity areas on T2-weighted images.

Statistical Analysis

Statistical analyses were performed by using StatView 5.0 software (SAS Institute, Cary, North Carolina). Between patients with LYH

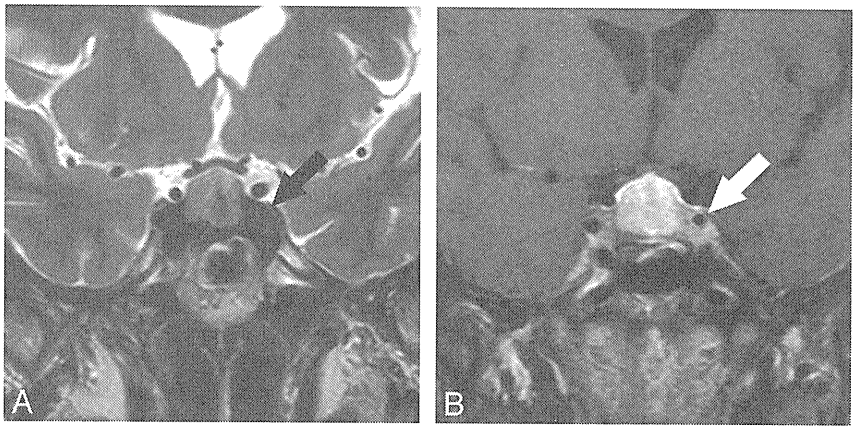

Fig 1. MR images of LYH (case 1) in a 38-year-old woman with partial hypopituitarism and diabetes insipidus. This patient had an 11-month history of headache, vomiting, polyuria, and polydipsia; transsphenoidal biopsy was performed and LYH proved histologically. *A*, Coronal T2-weighted image (TR/TE/NEX = 3500/120 ms/3) shows a large pituitary mass compressing the optic chiasm. A dark-signal-intensity area is seen in the cavernous sinus and sellar floor (*arrow*). *B*, Coronal contrast-enhanced T1-weighted image (TR/TE/NEX = 650/16 ms/3) shows a large pituitary mass with homogeneous enhancement. Bilateral cavernous sinuses are swollen, with poor enhancement. The left ICA in the left cavernous sinus is narrowed (*arrow*).

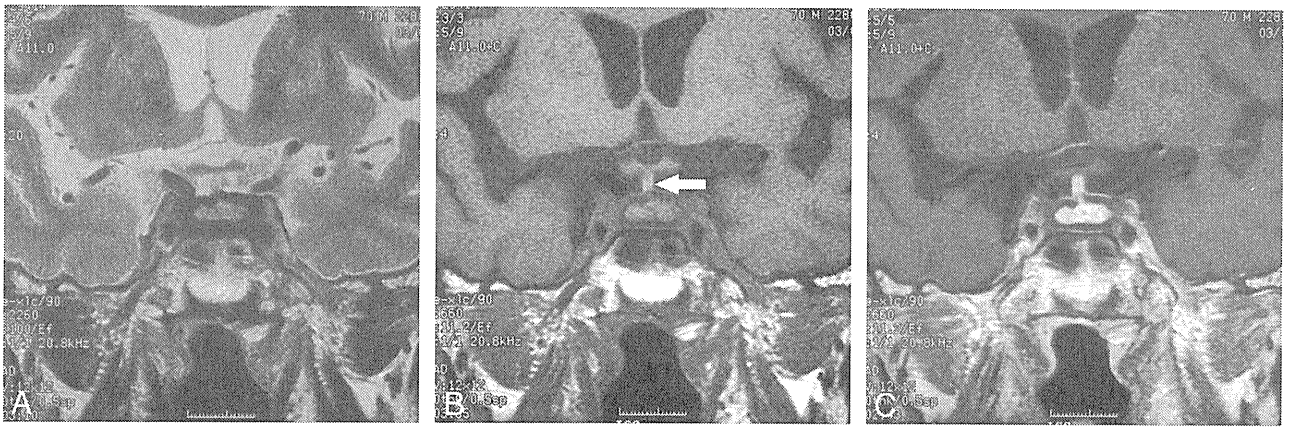

Fig 2. MR images of LYH (case 3) in a 70-year-old man with panhypopituitarism without diabetes insipidus. His chief complaint was general fatigue, and he was followed up for >5 years. Replacement therapy (glucocorticoid, levothyroxine) was performed. *A*, Coronal T2-weighted image (TR/TE/NEX = 2260/100 ms/3) shows the relatively large pituitary gland. A dark-signal-intensity area is seen around the pituitary gland. The inner portions of the bilateral cavernous sinuses show low signal intensity. *B*, Coronal T1-weighted image (TR/TE/NEX = 660/11.2 ms/3) shows the relatively large pituitary gland and stalk. A low-signal-intensity area is seen around the pituitary gland. The stalk shows high signal intensity, suggesting that it is storing antidiuretic hormone (*arrow*). *C*, Coronal contrast-enhanced T1-weighted image (TR/TE/NEX = 600/9.9 ms/3) shows homogeneous enhancement in the pituitary gland and the stalk. The area around the pituitary gland and bilateral cavernous sinuses shows poor enhancement.

and those with pituitary adenoma, each imaging finding as described above was compared by using the Fisher exact probability test. *P* values $< .05$ indicated statistical significance. We also calculated sensitivity and specificity for the diagnosis of LYH of each imaging finding as described above.

Results

Clinical findings for the 20 patients with LYH are summarized in On-line Table 1. Endocrinologic studies showed that 17 of 20 patients (85%) had some degree of hypopituitarism: panhypopituitarism or partial hypopituitarism with diabetes insipidus in 12 patients, only panhypopituitarism or partial hypopituitarism in 2 patients, and only diabetes insipidus in 3 patients.

Clinical findings for the 22 patients with pituitary adenoma are summarized in On-line Table 2. Endocrinologic studies showed partial hyperpituitarism and partial hypopituitarism in 3 patients, only partial hyperpituitarism in 7 patients, and only hypopituitarism in 1 patient. In 4 patients who had hormonal examination of the posterior lobe, none had diabetes insipidus.

MR imaging findings of the patients with LYH and pituitary adenoma are summarized in On-line Table 3. PPHI was absent in 17 patients (85%) with LYH and 3 (14%) with pituitary adenoma. Ectopic PPHI was seen in 1 patient with LYH and 3 with pituitary adenoma. Seventeen patients (85%) with LYH had thickened stalks. On the other hand, no patients (0%) with pituitary adenoma had thickened stalks, though in 2 patients with LYH and 4 with pituitary adenoma, the stalk was unclear due to pituitary tumoral compression. The pituitary gland was symmetric in 17 patients (85%) with LYH and in 2 (9%) with pituitary adenoma. Homogeneous enhancement was seen in 13 patients (65%) with LYH and in only 2 patients (9%) with pituitary adenoma. The dural tail was seen in 13 patients (65%) with LYH and 17 patients (77%) with pituitary adenoma. On T2-weighted images, parasellar dark-signal-intensity areas were seen in 7 patients (35%) with LYH (Figs 1–3); the other 13 patients with LYH showed isointensity. Parasellar low-signal-intensity areas were seen in 2 patients (9%) with pituitary adenoma (Fig 4), but no parasellar dark-signal-intensity areas were seen in any patients with pituitary adenoma.

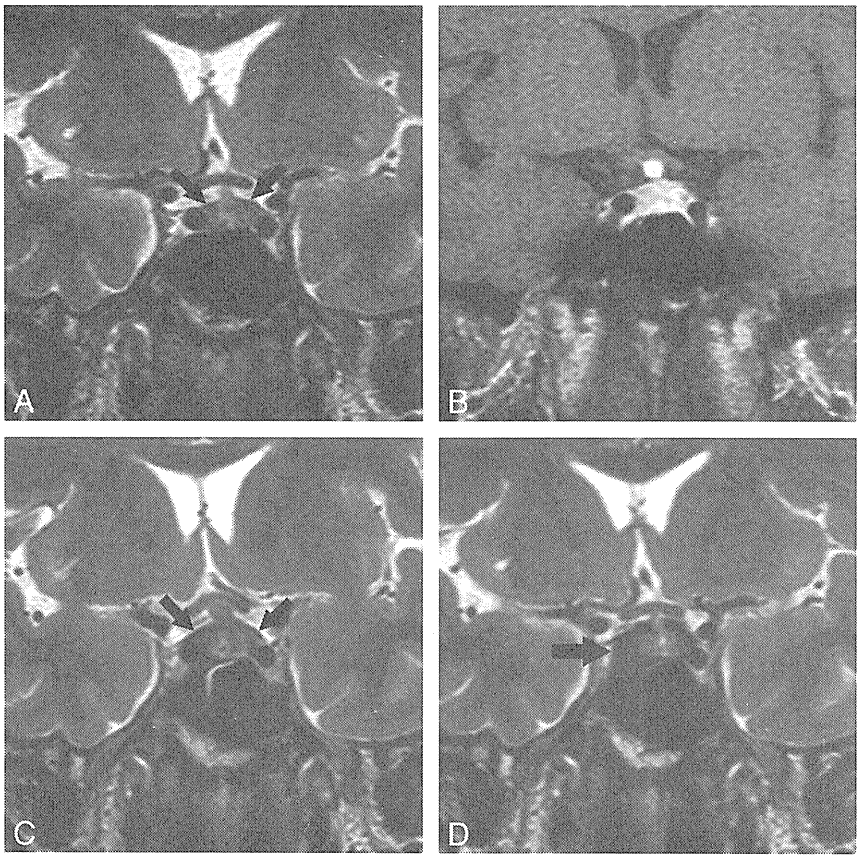

Fig 3. Serial MR images of LYH (case 4) in a 36-year-old man. Partial diabetes insipidus was observed in the early stage, and partial hypopituitarism was revealed later during the follow-up and treated by replacement therapy. *A,* The first coronal T2-weighted image (TR/TE/NEX = 3500/120 ms/3) shows the pituitary gland. Very thin dark-signal intensity areas on the upper edge of the pituitary gland (*arrows*) are seen. *B,* The first coronal contrast-enhanced T1-weighted image (TR/TE/NEX = 650/16 ms/3) shows a large pituitary gland with homogeneous enhancement. This section is slightly behind *A.* The large stalk with homogeneous enhancement slightly compresses the optic chiasm. *C,* The second coronal T2-weighted image (TR/TE/NEX = 3500/120 ms/3) 2 months after the first study shows a large pituitary gland and stalk. The previously noted thin dark-signal-intensity areas on the upper edge of the pituitary gland (*arrows*) were thicker than those in the first study. *D,* The third coronal T2-weighted image (TR/TE/NEX = 3500/120 ms/3) 8 months after the first study shows a large pituitary gland. The stalk is decreased in size. Dark-signal-intensity areas on the upper edge of the pituitary gland have thickened. The dark-signal-intensity area is enlarged and involves the right cavernous sinus; the right ICA in the cavernous sinus is narrower (*arrow*) than that in the previous study.

The other 20 patients with pituitary adenoma showed isointensity. On T1-weighted images, parasellar low-signal-intensity areas were seen in 2 patients (10%) with LYH. The other 18 patients with LYH showed isointensity. On the other hand, all patients with pituitary adenoma showed isointensity. Pituitary adenomas involved the cavernous sinuses in 11 patients; however, the cavernous sinuses were isointense with gray matter on T2- or T1-weighted images, and dark-signal-intensity areas were not seen.

Details of the MR imaging findings in the 7 patients who showed parasellar dark signal intensity on T2-weighted images are summarized in On-line Table 4. Dark-signal-intensity areas in the cavernous sinuses were seen in 6 patients. Cavernous sinuses were swollen in 4 patients (Figs 1 and 2). Enhancement of the cavernous sinuses after an intravenous injection of contrast medium was poor in 3 patients (Figs 1 and 2). ICAs in the cavernous sinuses were narrowed in 3 patients (Figs 1 and 3). In cases 4, 5, and 6, dark-signal-intensity areas in the cavernous sinus were not seen in the first MR imaging study but appeared 2–20 months later. On T2-weighted images, dark-signal-intensity bands around the anterior lobe and/or posterior lobe of the pituitary gland were seen in 4 patients (Fig 3). In case 5, this band was not seen in the first MR imaging study but appeared 20 months later. In case 4, a very thin dark-signal-intensity band was noted on the upper edge of the posterior gland in the first study and was thickened on follow-up studies 2 and 8 months later (Fig 3).

Between patients with LYH and those with pituitary adenoma, a significant difference was identified by statistical analysis for the number of patients with PPHI on T1-weighted images ($P < .0001$), thickened stalk ($P < .0001$), pituitary symmetry ($P < .0001$), homogeneous enhancement ($P = .0001$; we excluded the cases without contrast enhancement), and dark-signal-intensity areas on T2-weighted images ($P = .0015$). No significant difference was identified for the number of patients with the dural tail ($P = .36$; we excluded the cases without contrast enhancement) and low-signal-intensity areas on T1-weighted images ($P = .11$). Sensitivity and specificity for the diagnosis for LYH were as follows: 0.85 and 0.95 for the loss of PPHI; 0.85 and 0.82 for the thickened stalk; 0.85 and 0.91 for the pituitary symmetry; 0.68 and 0.91 for the homogeneous enhancement (we excluded the cases without contrast enhancement); 0.65 and 0.23 for the dural tail; and 0.35 and 1.00 for the dark-signal-intensity areas on T2-weighted images, and 0.10 and 1.00 for the low-signal-intensity areas on T1-weighted images around the sellar and parasellar areas.

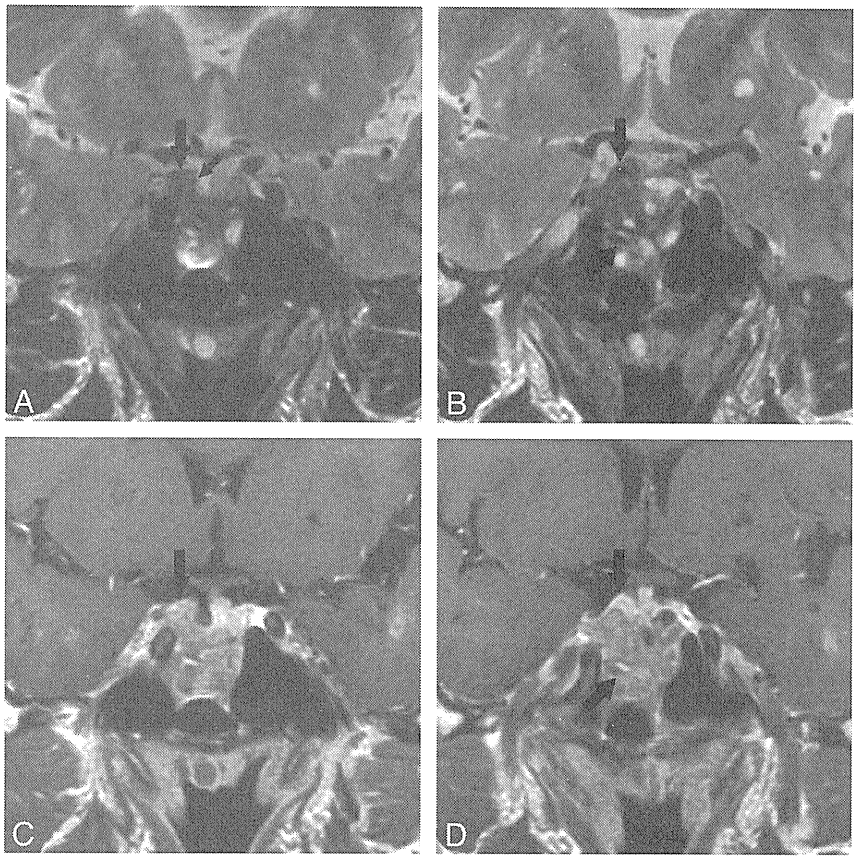

Fig 4. MR images of pituitary adenoma (case 5) in a 54-year-old woman. Acromegaly and partial hyperpituitarism were observed. She was treated with transsphenoidal resection, and the proved pathologic diagnosis was GH-secreting pituitary adenoma. *A* and *B*, Coronal T2-weighted images (TR/TE/NEX = 3500/120 ms/3) show a large pituitary mass destroying the sellar floor and extending in the sphenoid sinus. The upper portion of the mass is mixed low intensity, and the lower portion shows mixed high signals. Large arrows indicate small dark-signal-intensity areas in the pituitary mass. A low-signal-intensity margin is seen in the medial aspect of the upper pituitary mass (*small arrow*). *C* and *D*, Coronal contrast-enhanced T1-weighted images (TR/TE/NEX = 600/9.9 ms/3) show heterogeneous enhancement in the pituitary mass. Arrows indicate enhanced focal areas in the pituitary mass, which correspond to the dark-signal-intensities on the T2-weighted images in *A* and *B*.

Discussion

The present study reviewed a series of clinical and MR imaging findings in 20 patients with LYH. To the best of our knowledge, this study has reviewed original MR imaging findings in the largest number of patients with LYH. We demonstrated a new characteristic parasellar T2 dark sign (dark-signal-intensity area on T2-weighted images around the pituitary gland and in the cavernous sinus) in patients with LYH for the first time. Although sensitivity for the parasellar T2 dark sign was 0.35, lower than that for loss of PPHI, thickened stalk, pituitary symmetry, homogeneous enhancement, or the dural tail, specificity for the parasellar T2 dark sign was 1.00; and this finding was characteristic enough to distinguish with certainty the more common pituitary adenoma from LYH because false-positive cases were not found. T2-weighted images depicted the parasellar involvement of LYH well. Our results also suggest that there are variations of localization of T2 dark areas in LYH.

Some previous studies reported that loss of PPHI, thickened stalk, pituitary symmetry, homogeneous enhancement, and the dural tail were useful for distinguishing LYH from pituitary adenomas,[2,3,8,11-14] but only 1 previous study investigated this statistically. Gutenberg et al[14] reported that these findings contributed significantly to classifying the outcome as pituitary adenoma or autoimmune hypophysitis (including lymphocytic and granulomatous hypophysitis), and our results were consistent with their findings.[14]

Although MR imaging findings such as loss of PPHI, thickened stalk, pituitary symmetry, and homogeneous enhancement showed significant difference in the statistical analysis in the present study, these findings were nonspecific and were observed in both diseases. Loss of PPHI was observed in central diabetes insipidus due to idiopathic, inflammatory, or neoplastic processes, including pituitary adenoma.[8,18-23] The stalk was sometimes unclear due to pituitary tumoral compression. Pituitary symmetry or asymmetry depends on tumor size, location, or invading areas.[24] Cystic, necrotizing, or hemorrhagic changes also influence the enhancement pattern.[25] Cystic appearance was described in 5% of the patients with LYH.[1,8,11,12,26-34] Homogeneous enhancement can also be observed in pituitary adenomas.[35] On the other hand, parasellar T2 dark sign was a characteristic finding in LYH and can contribute to distinguishing pituitary LYH from adenoma with certainty.

Clinical findings revealed that panhypopituitarism or partial hypopituitarism was seen in 17 patients (85%) with LYH. On the other hand, partial hypopituitarism was seen in only 4 patients (18%) with pituitary adenoma. We think that hypopituitarism may be useful clinical information, suggesting LYH rather than pituitary adenoma. The endocrinologic man-

ifestation of LYH can vary widely, from only hyperprolactinemia, probably due to stalk compression, to panhypopituitarism mimicking Sheehan syndrome.[1] In a recent report, the hormones most frequently impaired were ACTH, followed by TSH, LH/FSH, and vasopressin in patients with LYH.[8] On the other hand, hypogonadism rather than hypocortisolemia or diabetes insipidus is usually the initial problem in pituitary adenoma.[4] In the present study, ACTH deficiency was seen in only 2 of 13 patients with LYH who had partial hypopituitarism, and insufficient hormones of the anterior pituitary lobe had some overlaps between pituitary adenoma and LYH. Isolated ACTH deficiency is not specific to LYH because it can be observed in the absence of LYH,[36] and isolated deficiencies of other anterior pituitary hormones have been described in LYH.[37] We think that MR imaging findings, in addition to endocrinologic studies, can play an important role in distinguishing pituitary adenoma from LYH.

In the previous reports, histopathologic analysis revealed that LYH is extensively infiltrated by lymphoplasmacytic cells, consisting of lymphocytes, plasma cells, and macrophages.[3] Lymphoplasmacytic aggregates surround the atrophic acini of pituitary cells, whereas the remaining pituitary tissue showed areas of reactive fibrosis.[26,38] Caturegli et al[8] reported that fibrosis was common (47% of 267 cases of LYH) and often severe in their pathologic review. We think that dark-signal-intensity areas on T2-weighted images around the pituitary gland and in the cavernous sinus reflected fibrotic changes accompanied by infiltration of lymphoplasmacytic cells. In the present study, the parasellar T2 dark signs were seen in the first MR imaging study in the 5 patients with LYH; however, this sign was not seen in the first MR imaging study of the 2 patients with LYH, but appeared 2–20 months after the first MR imaging study (On-line Table 4).

LYH is a chronic inflammatory disease that affects the pituitary gland and parasellar areas, and the duration of disease in patients with LYH is relatively long.[3] We think that fibrotic changes progressed in the clinical course of LYH and appeared as parasellar T2 dark signs. We also think that the sensitivity and specificity of the parasellar T2 dark sign may vary with time, and thus the parasellar T2 dark sign may not be useful for making an initial diagnosis. If the parasellar T2 dark sign was not seen in the initial MR imaging in patients who were suspected of the diagnosis of LYH, further follow-up MR imaging studies may be needed to detect the sign.

In the present study, cases 1 and 2 were diagnosed histologically by transsphenoidal biopsy. In case 2, biopsy specimens showed adenohypophysitis with focal lymphocytic infiltrate with lymphoid follicle formation and attached portions of attenuated hyalinized fibrous tissue; however, fibrous tissue was not found in case 1. We think the reason is that the biopsy specimens included only a small portion of the anterior lobes and did not include fibrous tissue. In the previous reports, approximately 10% of pituitary adenomas contained fibrosis.[39] Iuchi et al[40] reported that the signal intensities on T2-weighted images were significantly correlated with the percentage of collagen content of the pituitary adenomas, and adenomas that showed lower signal intensities on T2-weighted images contained more collagen. However, low signal intensities on T2-weighted images in pituitary adenomas are usually seen in the pituitary masses and not outside the masses in the parasellar areas. However, the histopathologic findings of LYH were characterized by massive infiltration of lymphocytes and plasma cells followed by necrosis or surrounding parenchymal fibrosis.[41] Therefore, the parasellar T2 dark sign is more suitable for LYH that infiltrates around the pituitary. Some previous studies have reported cavernous involvement in patients with LYH,[5,6,10,42-46] but no studies have mentioned the parasellar T2 dark sign.

In the present study, we focused on the parasellar T2 dark sign in the differential diagnosis between LYH and pituitary adenoma; however, other differential diagnoses for parasellar T2 dark sign should be considered in practical clinical cases. Some cases such as sarcoidosis, lymphoma, or Tolosa-Hunt syndrome could potentially have relatively low signal intensity on T2-weighted images and may show findings similar to those of the parasellar T2 dark sign, though we have no experience of such cases. In particular, sarcoidosis should be carefully considered because it sometimes causes secondary granulomatous hypophysitis,[4] and its differential diagnosis on MR imaging findings may be very difficult. We think that clinical presentation such as medical history and laboratory findings, in addition to MR imaging findings, needs to be investigated in detail in the diagnosis of LYH.

This study had several limitations. The first is that not all patients with LYH had pathologic confirmation; only 4 of 20 patients with LYH and only 2 of 7 patients with parasellar T2 dark sign had transsphenoidal biopsy. Additionally, there were 5 patients who had a history of autoimmune disease such as IgG4-related disorders, rheumatoid arthritis, and bullous pemphigoid. Other disorders, such as granulomatous hypophysitis or sarcoidosis, could feasibly have similar MR imaging findings. However, the duration of follow-up was relatively long (from 9 months to 9 years) in the 11 patients without pathologic confirmation or a history of autoimmune disease. Sarcoidosis is liable to recur not only in the intracranial area but also in the extracranial portion during longitudinal follow-up, but these 11 patients had no recurrence. In addition, they had no laboratory findings supporting sarcoidosis. Granulomatous hypophysitis is an extremely rare disorder (annual incidence of 1 in 10 million) and is usually diagnosed in postmortem specimens.[4,47] The other limitation was that the present study was retrospective; most of the patients had only had a routine pituitary MR imaging study. If we had been able to prospectively evaluate these patients by using dynamic contrast-enhanced MR imaging[5] or contrast-enhanced 3D constructive interference in the steady state,[48] more details of the sellar and parasellar structures and signal intensity would have been shown. Further prospective studies that compare the findings obtained from high-field MR imaging systems or long-term follow-up MR imaging with the histopathologic findings should be conducted.

Conclusions

MR imaging findings, such as loss of PPHI, thickened stalk, pituitary symmetry, homogeneous enhancement, and parasellar T2 dark sign, can contribute to distinguishing pituitary adenoma from LYH. The parasellar T2 dark sign in particular was a characteristic finding in patients with LYH, which was not observed in pituitary adenomas.

References

1. Thodou E, Asa SL, Kontogeorgos G, et al. **Lymphocytic hypophysitis: clinicopathological findings.** *J Clin Endocrinol Metab* 1995;80:2302–11
2. Powrie JK, Powell M, Ayers AB, et al. **Lymphocytic adenohypophysitis: magnetic resonance imaging features of two new cases and a review of the literature.** *Clin Endocrinol* 1995;42:315–22
3. Bellastella A, Bizzarro A, Coronella C, et al. **Lymphocytic hypophysitis: a rare or underestimated disease?** *Eur J Endocrinol* 2003;149:363–76
4. Rivera JA. **Lymphocytic hypophysitis: disease spectrum and approach to diagnosis and therapy.** *Pituitary* 2006;9:35–45
5. Sato N, Sze G, Endo K. **Hypophysitis: endocrinologic and dynamic MR findings.** *AJNR Am J Neuroradiol* 1998;19:439–44
6. Supler ML, Mickle JP. **Lymphocytic hypophysitis: report of a case in a man with cavernous sinus involvement.** *Surg Neurol* 1992;37:472–76
7. Imura H, Nakao K, Shimatsu A, et al. **Lymphocytic infundibuloneurohypophysitis as a cause of central diabetes insipidus.** *N Engl J Med* 1993;329:683–89
8. Caturegli P, Newschaffer C, Olivi A, et al. **Autoimmune hypophysitis.** *Endocr Rev* 2005;26:599–614
9. Leung GK, Lopes MB, Thorner MO, et al. **Primary hypophysitis: a single-center experience in 16 cases.** *J Neurosurg* 2004;101:262–71
10. Nussbaum CE, Okawara S, Jacobs LS. **Lymphocytic hypophysitis with involvement of the cavernous sinus and hypothalamus.** *Neurosurgery* 1991;28:440–44
11. Saiwai S, Inoue Y, Ishihara T, et al. **Lymphocytic adenohypophysitis: skull radiographs and MRI.** *Neuroradiology* 1998;40:114–20
12. Ahmadi J, Meyers GS, Segall HD, et al. **Lymphocytic adenohypophysitis: contrast-enhanced MR imaging in five cases.** *Radiology* 1995;195:30–34
13. Chelaifa K, Bouzaidi K, Harzallah F, et al. **Lymphocytic hypophysitis.** *J Neuroradiol* 2002;29:57–60
14. Gutenberg A, Larsen J, Lupi I, et al. **A radiologic score to distinguish autoimmune hypophysitis from nonsecreting pituitary adenoma preoperatively.** *AJNR Am J Neuroradiol* 2009;30:1766–72
15. Kucharczyk W, Davis DO, Kelly WM, et al. **Pituitary adenomas: high resolution MR imaging at 1.5 T.** *Radiology* 1986;161:761–5
16. Leggett DA, Hill PT, Anderson RJ. **'Stalkitis' in a pregnant 32-year-old woman: a rare cause of diabetes insipidus.** *Australas Radiol* 1999;43:104–07
17. Johnsen DE, Woodruff WW, Allen IS, et al. **MR imaging of the sellar and juxtasellar regions.** *Radiographics* 1991;11:727–58
18. Terano T, Seya A, Tamura Y, et al. **Characteristics of the pituitary gland in elderly subjects from magnetic resonance imaging: relationship to pituitary hormone secretion.** *Clin Endocrinol (Oxf)* 1996;45:273–79
19. Fujisawa I, Nishimura K, Asato R, et al. **Posterior lobe of the pituitary in diabetes insipidus: MR findings.** *J Comput Assist Tomogr* 1987;11:221–25
20. Sato N, Ishizaka H, Matsumoto M, et al. **MR detectability of posterior pituitary high signal and direction of frequency encoding gradient.** *J Comput Assist Tomogr* 1991;15:355–58
21. Sato N, Ishizaka H, Yagi H, et al. **Posterior lobe of the pituitary in diabetes insipidus: dynamic MR imaging.** *Radiology* 1993;186:357–60
22. Sato N, Endo K, Ishizaka H, et al. **Serial MR intensity changes of the posterior pituitary in a patient with anorexia nervosa, high serum ADH, and oliguria.** *J Comput Assist Tomogr* 1993;17:648–50
23. Sato N, Endo K, Kawai H, et al. **Hemodialysis: relationship between signal intensity of the posterior pituitary gland at MR imaging and level of plasma antidiuretic hormone.** *Radiology* 1995;194:277–80
24. Chong BW, Kucharczyk W, Singer W, et al. **Pituitary gland MR: a comparative study of healthy volunteers and patients with microadenomas.** *AJNR Am J Neuroradiol* 1994;15:675–79
25. Bonneville JF, Bonneville F, Cattin F. **Magnetic resonance imaging of pituitary adenomas.** *Eur Radiol* 2005;15:543–48
26. Fehn M, Sommer C, Ludecke DK, et al. **Lymphocytic hypophysitis: light and microscopic findings and correlation to clinical appearance.** *Endocr Pathol* 1998;9:71–78
27. Sandler R, Danks KR, Hennigan SH, et al. **The widening spectrum of lymphocytic hypophysitis.** *J Ark Med Soc* 1998;95:197–200
28. Ishihara T, Hino M, Kurahachi H, et al. **Long-term clinical course of two cases of lymphocytic adenohypophysitis.** *Endocr J* 1996;43:433–40
29. McDermott MW, Griesdale DE, Berry K, et al. **Lymphocytic adenohypophysitis.** *Can J Neurol Sci* 1988;15:38–43
30. Farah JO, Rossi M, Foy PM, et al. **Cystic lymphocytic hypophysitis, visual field defects and hypopituitarism.** *Int J Clin Pract* 1999;53:643–44
31. Tamiya A, Saeki N, Kubota M, et al. **Unusual MRI findings in lymphocytic hypophysitis with central diabetes insipidus.** *Neuroradiology* 1999;41:899–900
32. Flanagan DE, Ibrahim AE, Ellison DW, et al. **Inflammatory hypophysitis: the spectrum of disease.** *Acta Neurochir (Wien)* 2002;144:47–56
33. Lee SJ, Yoo HJ, Park SW, et al. **A case of cystic lymphocytic hypophysitis with cacosmia and hypopituitarism.** *Endocr J* 2004;51:375–80
34. Pérez-Núñez A, Miranda P, Arrese I, et al. **Lymphocytic hypophysitis with cystic MRI appearance.** *Acta Neurochir (Wien)* 2005;147:1297–300
35. Heshmati HM, Kujas M, Casanova S, et al. **Prevalence of lymphocytic infiltrate in 1400 pituitary adenomas.** *Endocr J* 1998;45:357–61
36. Nagai Y, Ieki Y, Ohsawa K, et al. **Simultaneously found transient hypothyroidism due to Hashimoto's thyroiditis, autoimmune hepatitis and isolated ACTH deficiency after cessation of glucocorticoid administration.** *Endocr J* 1997;44:453–8
37. Barkan AL, Kelch RP, Marshall JC. **Isolated gonadotrope failure in the polyglandular autoimmune syndrome.** *N Engl J Med* 1985;312:1535–40
38. Durán Martınez M, Santonja C, Pavon de Paz I, et al. **Lymphocytic hypophysitis: report of an unusual case of a rare disorder.** *J Endocrinol Invest* 2001;24:190–93
39. Wang H, Li WS, Shi DJ, et al. **Correlation of MMP(1) and TIMP (1) expression with pituitary adenoma fibrosis.** *J Neurooncol* 2008;90:151–56
40. Iuchi T, Saeki N, Tanaka M, et al. **MRI prediction of fibrous pituitary adenomas.** *Acta Neurochir (Wien)* 1998;140:779–86
41. Nishioka H, Ito H, Miki T, et al. **A case of lymphocytic hypophysitis with massive fibrosis and the role of surgical intervention.** *Surg Neurol* 1994;42:74–78
42. Kartal I, Yarman S, Tanakol R, et al. **Lymphocytic panhypophysitis in a young man with involvement of the cavernous sinus and clivus.** *Pituitary* 2007;10:75–80
43. Melgar MA, Mariwalla N, Gloss DS, et al. **Recurrent lymphocytic hypophysitis and bilateral intracavernous carotid artery occlusion: an observation and review of the literature.** *Neurol Res* 2006;28:177–83
44. Lecube A, Francisco G, Rodríguez D, et al. **Lymphocytic hypophysitis successfully treated with azathioprine: first case report.** *J Neurol Neurosurg Psychiatry* 2003;74:1581–83
45. Tubridy N, Saunders D, Thom M, et al. **Infundibulohypophysitis in a man presenting with diabetes insipidus and cavernous sinus involvement.** *J Neurol Neurosurg Psychiatry* 2001;71:798–801
46. Nakamura Y, Okada H, Wada Y, et al. **Lymphocytic hypophysitis: its expanding features.** *J Endocrinol Invest* 2001;24:262–67
47. Cheung CC, Ezzat S, Smyth HS, et al. **The spectrum and significance of primary hypophysitis.** *J Clin Endocrinol Metab* 2001;86:1048–53
48. Yagi A, Sato N, Taketomi A, et al. **Normal cranial nerves in the cavernous sinuses: contrast-enhanced three-dimensional constructive interference in the steady state MR imaging.** *AJNR Am J Neuroradiol* 2005;26:946–50

Neuroradiology (2010) 52:1101–1109
DOI 10.1007/s00234-010-0690-9

DIAGNOSTIC NEURORADIOLOGY

Added value of contrast-enhanced CISS imaging in relation to conventional MR images for the evaluation of intracavernous cranial nerve lesions

Akiko Yagi · Noriko Sato · Ayako Takahashi · Hideo Morita · Makoto Amanuma · Keigo Endo · K. Takeuchi

Received: 30 November 2009 / Accepted: 18 March 2010 / Published online: 10 April 2010

Abstract
Introduction The normal cranial nerves (CNs) of the cavernous sinus can be clearly demonstrated using contrast-enhanced constructive interference in steady-state (CISS) magnetic resonance imaging (MRI). This study used the method to evaluate pathological CNs III, IV, V_1, V_2, and VI in cavernous sinuses affected by inflammatory and neoplastic diseases.
Methods MR images from 17 patients with diseases involving the cavernous sinuses and/or causing neuropathy in CNs III–VI were retrospectively evaluated. The patients were divided into inflammatory (n=11) and neoplastic (n=6) groups. We defined CNs as abnormal when they exhibited enlargement or enhancement. CNs were evaluated using both contrast-enhanced CISS and T1-weighted MRI.
Results In the inflammatory group, abnormal CNs were identified by contrast-enhanced CISS MRI in 13 of 25 symptomatic CNs (52%) in eight patients, but in only two CNs (8%) in two patients by contrast-enhanced T1-weighted MRI. In the neoplastic group, both sequences of contrast-enhanced CISS and T1-weighted MRI detected abnormalities in the same three of eight symptomatic CNs (37.5%), i.e., the three CNs were all in the same patient with adenoid cystic carcinoma.
Conclusion Contrast-enhanced CISS MRI is useful for detecting CN abnormalities in inflammatory pathological conditions of the cavernous sinuses.

Keywords Cranial nerves · Cavernous sinus · Constructive interference in steady state · Magnetic resonance imaging

A. Yagi · A. Takahashi · H. Morita · M. Amanuma · K. Endo
Department of Diagnostic Radiology and Nuclear Medicine,
Gunma University School of Medicine,
Gunma, Japan

N. Sato (✉)
Department of Radiology,
National Center Hospital of Neurology and Psychiatry,
4-1-1 Ogawahigashi-chyo,
Kodaira, Tokyo 187-8551, Japan
e-mail: snoriko@ncnp.go.jp

K. Takeuchi
Department of Health and Welfare,
Takasaki University of Health and Welfare,
Gunma, Japan

Introduction

The cavernous sinus is a clinically important structure that contains the internal carotid arteries and cranial nerves (CNs) III (oculomotor nerve), IV (trochlear nerve), V_1 (ophthalmic nerve), V_2 (maxillary nerve), and VI (abducens nerve). Involvement of the cavernous sinuses in various diseases (e.g., Tolosa-Hunt syndrome) or direct invasion by malignancy can be accompanied by multiple cranial neuropathies. However, it has remained difficult to detect CN morphological abnormalities. Although several studies have reported the characteristics of cavernous sinus diseases in magnetic resonance imaging (MRI) [1–11], the precise imaging study evaluation of abnormal CNs in the cavernous sinuses has remained almost impossible to date.

Three-dimensional (3D) constructive interference in steady-state (CISS) MRI is an approach using a high spatial resolution, refocused gradient-echo sequence, which is flow-compensated. The 3D CISS sequence depicts small structures surrounded by cerebrospinal fluid (CSF) with high contrast and high spatial resolution and is therefore

suitable for depicting all CNs passing through the cistern [12]. This method is also useful for demonstrating fine structures in the cavernous sinus if gadolinium-diethylenetriaminepentaacetate (Gd-DTPA) is injected [13]. A previous study has shown that normal CNs passing through the cavernous sinus are well demonstrated in vivo on 3D CISS MRI after injection of Gd-DTPA because the well-enhanced venous plexus of the cavernous sinus plays a role in imaging similar to that of the CSF [14]. In that study, contrast-enhanced 3D CISS MRI was found to be superior to contrast-enhanced T1-weighted imaging for the depiction of normal CNs in cavernous portions of the sinus. We therefore hypothesized that contrast-enhanced 3D CISS MRI would also be superior to contrast-enhanced T1-weighted MRI for detecting pathological CNs of the cavernous sinuses. In the present study, we evaluated the CNs of patients with inflammatory and neoplastic diseases involving the cavernous sinuses by both contrast-enhanced 3D CISS and contrast-enhanced T1-weighted MRI to evaluate the usefulness of contrast-enhanced 3D CISS when considered in conjunction with the clinical findings.

Materials and methods

Patients

We retrospectively studied MR images of 26 patients obtained from 2002 to 2007 at our hospital. The patients' clinical information was obtained by MR inspection requests submitted by attending physicians prior to MR examination. Based on this information, we selected patients in whom the disease was suspected to be located around the cavernous sinuses, and detailed MR examination focusing on the cavernous sinuses was performed. Thirteen patients had inflammatory disease and 13 patients had neoplasms involving the cavernous sinuses. Physical examination of all patients, including assessment of CN dysfunction, was performed by neurologists or neurosurgeons. Institutional Review Board approval was obtained for the study.

In the inflammatory group, two of 13 cases were excluded due to prominent motion artifacts upon MR examination. The characteristics of the remaining 11 patients with inflammatory diseases is shown in Table 1. Tolosa-Hunt syndrome, idiopathic meningitis, and neuritis were diagnosed based on clinical and imaging findings. One patient with fungal infection had an epidural abscess adjacent to the cavernous sinus, which was diagnosed at surgery. In the patient with allergic granulomatous angitis, the cavernous sinuses were involved due to internal carotid arteritis, and the diagnosis was made by skin biopsy (Table 1).

In the neoplastic group, seven of 13 cases were excluded from this study for the following reasons: five patients were postoperative, one patient had undergone irradiation therapy of the brain, and one patient had no pathologic confirmation because the tumor was considered benign, as it had remained stable (i.e., without growth) for 7 years. The patient who had received irradiation was excluded because such treatment can induce signal intensity changes in the cavernous sinus as a result of fibrosis, which may render identification of the CNs difficult. The remaining six pathologically demonstrated neoplasms in six patients were included in the neoplastic group (Table 2). A total of 17 patients (seven men and 10 women; mean age, 57.9 years; age range, 15 to 82 years) were included in the inflammatory and neoplastic groups combined.

MR protocol and assessment

All MR examinations were performed using a 1.5-T unit (Magnetom Symphony; Siemens, Erlangen, Germany) with a head coil. The intravenous contrast agent of gadopentetate dimeglumine was administered at a dose of 0.1 mmol/kg body weight. Precontrast coronal T1-weighted images and axial or coronal T2-weighted images were performed in all patients. All patients underwent contrast-enhanced 3D CISS MRI. Sixteen out of 17 patients underwent contrast-enhanced coronal conventional 2D T1-weighted images with or without fat suppression. The remaining one patient (case 9 in the inflammatory group) underwent contrast-enhanced T1-contrast 3D fast low angle shot (FLASH) echo examination. Contrast-enhanced 2D or 3D T1-weigted images had been obtained before 3D CISS images were scanned. The following pulse sequences were used: (a) conventional coronal T1-weighted images (450/15 [TR/TE], 200×180-mm field of view, 320×202 matrix, 3.0-mm section thickness, 0-mm intersection gap); (b) coronal T2-weighted images (4,000/108 [TR/TE], 200×180-mm field of view, 230×256 matrix, 3.0-mm section thickness, 0-mm intersection gap); (c) axial T2-weighted images (4,000/108 [TR/TE], 200×180-mm field of view, 230×256 matrix, 4.0-mm section thickness, 0.6-mm intersection gap); (d) 3D CISS (11.84/5.92 [TR/TE], 70° flip angle, 180×180-mm field of view, 39.2-mm slab thickness, 256×224 matrix, 56 3D partitions, one slab, 0.7×0.8-mm pixel size, 0.7-mm effective section thickness, one signal acquired, and imaging time of 4 min 28 s); (e) 3D FLASH (20/4.93 [TR/TE], 25° flip angle, 220×220-mm field of view, 70.4-mm slab thickness, 205×256 matrix, 64 3D partitions, one slab, 1.1×0.9-mm pixel size, 1.1-mm effective section thickness, one signal acquired, and imaging time of 4 min 22 s). Data obtained using 3D CISS (in all patients) and T1-weighted FLASH (only in case 9 of the inflammatory group) images were reconstructed in the coronal plane using section thicknesses of 0.7 and 1.1 mm, respectively. Images were analyzed using a multiplanar reconstruction program (Siemens).

Table 1 Clinical characteristics and MR imaging findings in patients with cavernous sinuses inflammation.

Patient no.	Age (years)/sex	Clinical characteristics			MR findings				
		Clinical diagnosis	Pathology	Cranial neuropathy	Cavernous Sinus			Location of dural enhancement	Other findings
					Cranial nerve abnormalities (enlargement and/or enhancement)		Swelling		
					CISS[a]	T1WI[a]			
1	55/M	Tolosa-Hunt syndrome	Not obtained	RIII, IV, V_1, VI	RIII	RIII	N	R frontal basal skull	N
2	72/M	Hypertrophic meningitis	Not obtained	LVI	LVI	LVI	N	Diffuse, L dominant	N
3	37/F	Angitis of both ICA	Allergic granulomatous angitis	LV_1, V_2, VI	N	N	Y	N	L ICA occlusion, L MC mass
4	64/F	Tolosa-Hunt syndrome	Not obtained	LIII, IV, VI	N	N	Y	N	N
5	60/M	Abducens neuritis	Not obtained	LVI	LVI	N	N	N	N
6	69/F	Focal meningitis	Not obtained	RIII	RIII	N	Y	R frontal basal skull	N
7	60/F	Tolosa-Hunt syndrome	Not obtained	RIII, V_1, V_2, VI	RIII, V_1, V_2, VI	N	Y	N	N
8	53/F	Tolosa-Hunt syndrome	Not obtained	LIII, IV	LIII, IV, V_1, V_2, VI	N	N	L frontal basal skull	N
9	82/F	Fungal infection	Fungal infection	LIII, V_1	N	N	Y	L frontal basal skull	N
10	15/F	Trigeminal neuritis	Not obtained	LV_1, V_2	LV_1, V_2	N	N	N	N
11	56/M	Tolosa-Hunt syndrome	Not obtained	RIII, IV	RIII	N	N	N	N

CISS constructive interference in steady state, *T1WI* T1-weighted imaging, *ICA* internal carotid artery, *N* not identified, *Y* observed, *MC* Meckel's cave, *R* right, *L* left

[a] With Gd-DTPA enhancement

Table 2 Clinical characteristics and MR imaging findings in patients with cavernous sinuses neoplasms.

Patient no.	Age (years)/sex	Clinical characteristics			MR findings				
		Diagnosis	Origin of neoplasm	Cranial neuropathy	Cavernous sinus			Location of dural enhancement	Other findings
					Cranial nerve abnormalities (enlargement and/or enhancement)		Swelling		
					CISS[a]	T1WI[a]			
1	54/M	Squamous cell carcinoma	Nasopharynx	LIII, IV VI	N	N	Y	Bilateral frontal basal skull	N
2	56/M	Lymphoma	Clivus	LVI	N	N	Y	N	N
3	64/F	Adenoid cystic carcinoma	R maxillary sinus	RIII, V_1, VI	RIII, IV, V_1, V_2, VI	RIII, IV, V_1, VI	N	R frontal basal skull	RV_2 swelling Enhancement of R foramen rotundum R maxillary sinus mass
4	76/F	Papillary carcinoma	Thyroid	LIII	N	N	Y	N	L MC invasion
5	58/F	Meningioma	Parasellar area	None	N	N	Y	L middle and both frontal basal skull	L MC invasion
6	53/M	Meningioma	Petroclival area	None	N	N	Y	N	L MC invasion

CISS constructive interference in steady state, *T1WI* T1-weighted imaging, *N* not identified, *Y* observed, *MC* Meckel's cave, *R* right, *L* left

[a] With Gd-DTPA enhancement

All MRI findings were visual assessed by two neuroradiologists (A.Y. and N.S., with 9 and 22 years of experience with MR, respectively). Both readers were blind to all clinical information regarding cranial neuropathy. Both neuroradiologists arrived at initial evaluations independently, and then any disagreement regarding final conclusions was resolved by consensus. The CNs were defined as abnormal when enlargement or enhancement on reconstructed contrast-enhanced coronal CISS or T1-weighted images was seen. Nerve enlargement was judged on the basis of a study of normal nerves [14]. Nerve enhancement was determined for comparison with the contralateral CN III, since the detectability of the normal CN III was reported to be 100% on both contrast-enhanced CISS and T1-weighted images [14]. We defined CNs III, IV, V_1, V_2, and VI as abnormal when the above-mentioned findings were observed on more than three consecutive sections of contrast-enhanced 3D CISS and T1-weighted FLASH images and on more than one section of contrast-enhanced conventional T1-weighted images because the thickness of the reconstructed 3D images ranged from 0.7 to 1.1 mm, whereas the thickness of the conventional 2D T1-weighted images was 3 mm. In cases in which CNs could not be identified individually, the CNs were not included as abnormal, as it would be difficult to differentiate pathological involvement of the CNs from just obscure without pathological involvement due to tight attachment to the mass or inflammatory areas. Interobserver agreement of interhemispheric enlargement and abnormal enhancement of the cranial nerves (kappa coefficient) was 0.51 ($p<0.01$), and the results were thus considered reliable. In addition to performing an assessment of the CNs, we also evaluated enhancement pattern of the cavernous sinus and cavernous sinus swelling, dural enhancement, and other additional findings (Tables 1 and 2).

Results

Inflammatory disease

The clinical characteristics and MRI findings of 11 patients in the inflammatory group were summarized in Table 1. All patients exhibited neuropathy of CNs III to VI. A total of 25 CNs exhibited neuropathy: CN III, $n=7$; CN IV, $n=4$; CN V_1, $n=5$; CN V_2, $n=3$; and CN VI, $n=6$.

On contrast-enhanced CISS images, 13 of the symptomatic 25 CNs were found to be abnormal (52%; Figs. 1a, 2a, and 3a) in eight cases. Nerve enlargement and enhancement were simultaneously observed. Among the 25 symptomatic CNs, abnormal CN imaging findings were seen in 71% (5/7) of CN III, 25% (1/4) of CN IV, 40% (2/5) of CN V_1, 67% (2/3) of CN V_2, and 50% (3/6) of CN VI.

On contrast-enhanced T1-weighted images, an enlargement of the CNs was observed in only two CNs of two cases

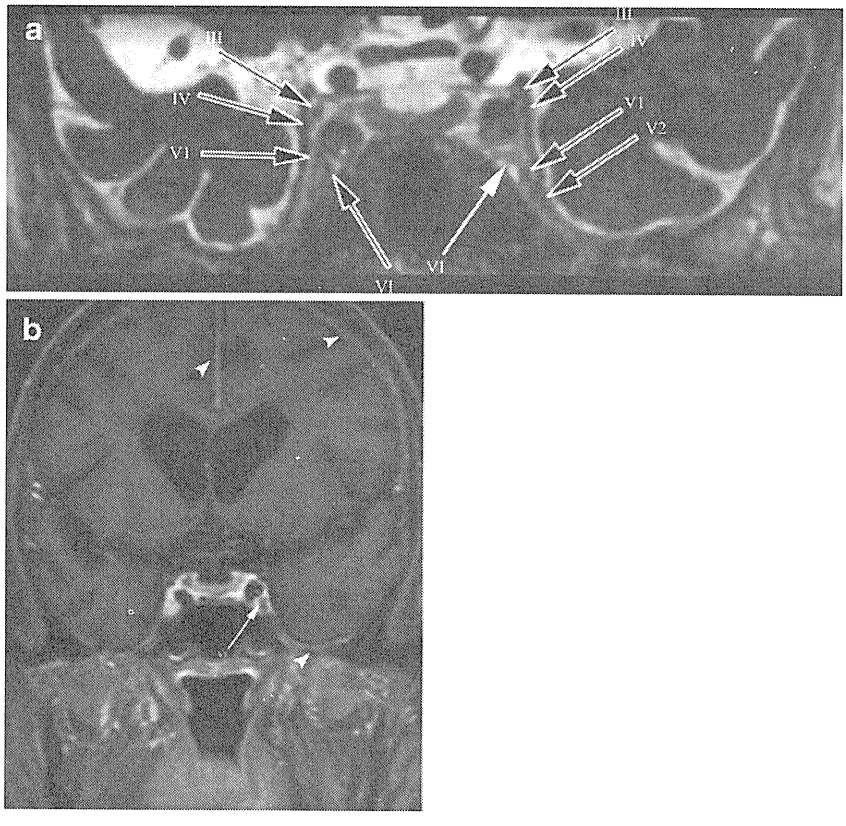

Fig. 1 Case 2 in the inflammatory group. A 72-year-old man with hypertrophic meningitis with neuropathy of left cranial nerve (CN) VI. **a** Contrast-enhanced coronal CISS MRI (11.8/5.9) reveals left CNs VI (*white arrow*) with enlargement and enhancement. Bilateral CNs III, IV, V_1, left V_2, and right CN VI appear normal (*black arrows*). Right CN V_2 is not detected. **b** Contrast-enhanced coronal T1-weighted MRI with fat suppression (450/15) reveals an abnormality of left CNs VI (*white arrow*). Diffuse dural enhancement is seen (*white arrowheads*)

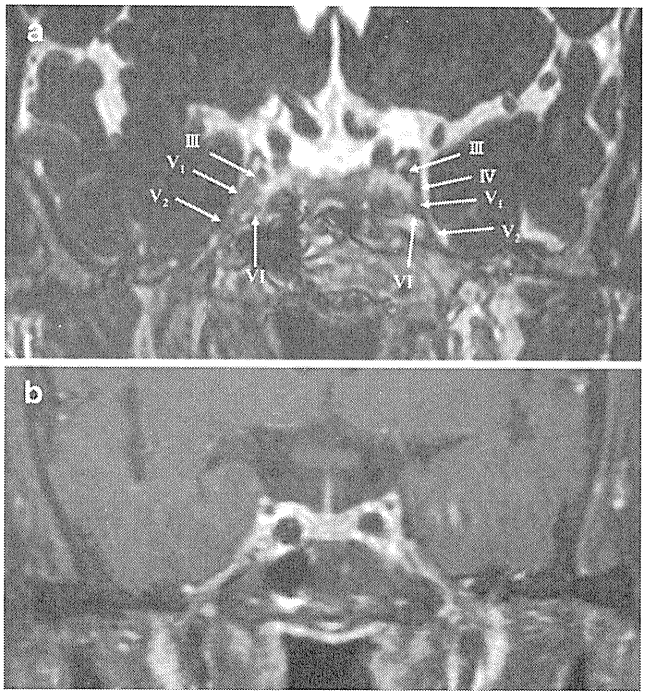

Fig. 2 Case 7 in the inflammatory group. A 60-year-old woman with Tolosa-Hunt syndrome with neuropathy of right cranial nerves (CNs) III and V_1, V_2, and VI. **a** Contrast-enhanced coronal CISS MRI (11.8/5.9) reveals right CNs III, V_1, V_2, and VI (*white arrows*) with enlargement and enhancement. Left cavernous sinus is normally enhanced and normal CNs III, IV, V_1, V_2, and VI are detected (*white arrows*). **b** Contrast-enhanced coronal T1-weighted MRI with fat suppression (450/15) shows any abnormalities

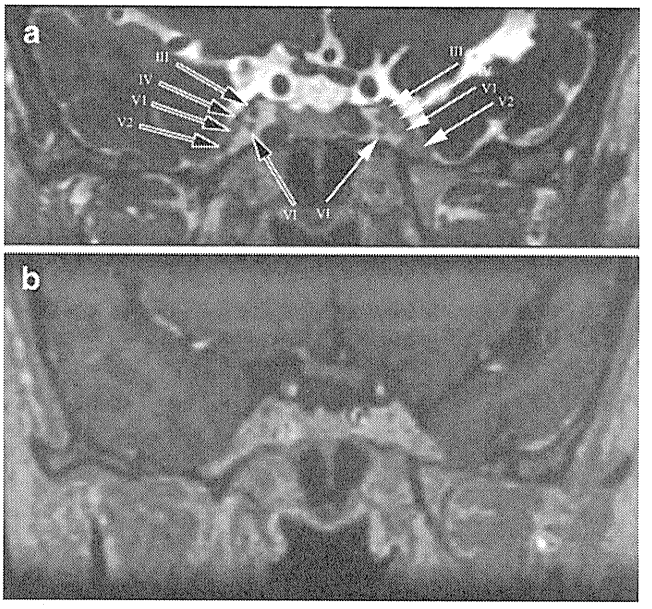

Fig. 3 Case 8 in the inflammatory group. A 53-year-old woman with Tolosa-Hunt syndrome with neuropathy of left cranial nerves (CNs) III and IV. **a** Contrast-enhanced coronal CISS MRI (TR/TE=11.8/5.9) reveals left CNs III, IV, V_1, V_2, and VI (*white arrows*) with enlargement and enhancement. Right CNs III–VI are normal (*black arrows*). **b** Contrast-enhanced FLASH MRI (450/15). Bilateral cavernous sinuses are almost symmetrical. No abnormality of the left intracavernous cranial nerves is identified

(cases 1 and 2; Fig. 1b) among the 25 symptomatic CNs (8%). Among these symptomatic CNs, abnormal CN imaging findings were seen in 14% (1/7) of CN III and 20% (1/5) of CN IV. No imaging abnormalities were detected in the other CNs.

Ipsilateral cavernous sinus was swelling in five out of 11 cases, and in two cases, cases 3 and 9, it was poorly enhanced compared to the contralateral one. In case 9, the upper and lateral part of the left cavernous sinus was poorly enhanced which obscured left CNs except for V_2 (Fig. 4a) on contrast-enhanced CISS images. But it was difficult to point it out on contrast-enhanced T1-weighted images. In case 3, the swelling whole left cavernous sinus was poorly enhanced on contrast-enhanced CISS images. But contrast-enhanced T1-weighted images did not detect it. In other cases, symmetrical cavernous sinus enhancement was shown.

Neoplastic disease

The clinical characteristics and MRI findings in the neoplastic cases were summarized in Table 2. Four of six patients in the neoplastic group demonstrated clinical neuropathy in eight CNs: CN III, n=3; CN IV, n=1; CN V_1, n=1; and CN VI, n=3.

On contrast-enhanced CISS images, abnormal findings among CNs were observed in only one patient (case 3) with adenoid cystic cancer (Fig. 5a). Three of the eight symptomatic CNs were found to be abnormally enlarged and enhanced (38%), and these three CNs were in the same patient. In the other five patients, no abnormal findings were detected. Among the eight symptomatic CNs, abnormal CN imaging findings were seen in 33% (1/3) of CN III, 25% (1/4) of CN IV, 100% (1/1) of CN V_1, and 33% (1/3) of CN VI.

Contrast-enhanced T1-weighted images also revealed enlargement of the same three CNs (38%) detected as abnormalities by CISS in the same patient (Fig. 5b). Among the eight symptomatic CNs, abnormal CN imaging findings were observed in 33% (1/3) of CN III, 25% (1/4) of CN IV, 100% (1/1) of CN V_1, and 33% (1/3) of CN VI.

In all cases except for case 3, unilateral or bilateral cavernous sinuses were swelling and poorly enhanced on both contrast-enhanced CISS and contrast-enhanced T1-weighted images. In case 4, contrast-enhanced CISS images revealed poor enhancement of the left whole cavernous sinus which obscured CNs, but right normally enhanced cavernous sinus detected CNs well (Fig. 6a). On the other hand, contrast-enhanced T1-weighted images just showed swelling of left cavernous sinus with partially poorly enhanced area.

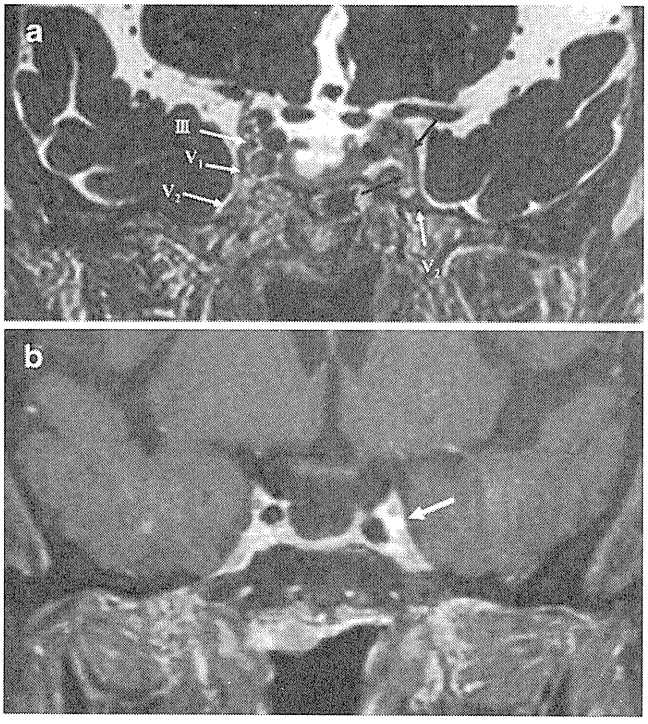

Fig. 4 Case 9 in the inflammatory group. A 82-year-old woman with fungal infection with neuropathy of left cranial nerves (CNs) III and V_1. **a** Contrast-enhanced coronal CISS MRI (11.8/5.9) reveals poorly enhanced area at the upper and lateral portion of the left cavernous (*black arrows*) which obscure left CNs except for V_2 (*white arrow*). Right cavernous sinus is normally enhanced and normal CNs III, IV, V_1, and V_2 are detected (*white arrows*). **b** Contrast-enhanced coronal T1-weighted MRI with fat suppression (450/15) does not show any abnormalities except for focal strong enhanced area at the upper portion of the left cavernous sinus (*white arrow*)

Discussion

In this study, we demonstrated that the use of the contrast-enhanced 3D CISS sequence clearly enabled the detection of CN abnormalities within the pathological cavernous sinuses in cases of pathology. Such CN abnormalities were more clearly detected on contrast-enhanced CISS than on T1-weighted images in cases of inflammatory disease, with an exception of the neoplastic group. However, the imaging quality of the intracavernous component was substantially clearer with the use of the 3D CISS sequence in each case, as shown in the figures. This is the first study to identify pathological CNs in the cavernous sinus using the contrast-enhanced 3D CISS sequence.

There are several reports of abnormal findings detected in the cavernous sinus on MR or CT imaging studies (e.g., enlargement of the cavernous sinus by tumor invasion and delayed enhancement of the cavernous sinus on dynamic MR study in patients with Tolosa-Hunt syndrome) [9, 15–17]. In cases of tumor invasion, CNs in the cavernous sinus can be obscure on enhanced MR images [15, 16]. It has also remained difficult to detect abnormal CNs using conventional methods, even when dynamic studies are included. Yagi et al. reported that contrast-enhanced 3D CISS images depicted the intracavernous segments of normal CNs III, IV, V_1, V_2, and VI in 100%, 61%, 92%, 88%, and 96% of 76 subjects, respectively. Moreover, in a comparative study of contrast-enhanced 3D CISS and contrast-enhanced T1-weighted images, the former had a significantly higher detection rate for all CNs except CN

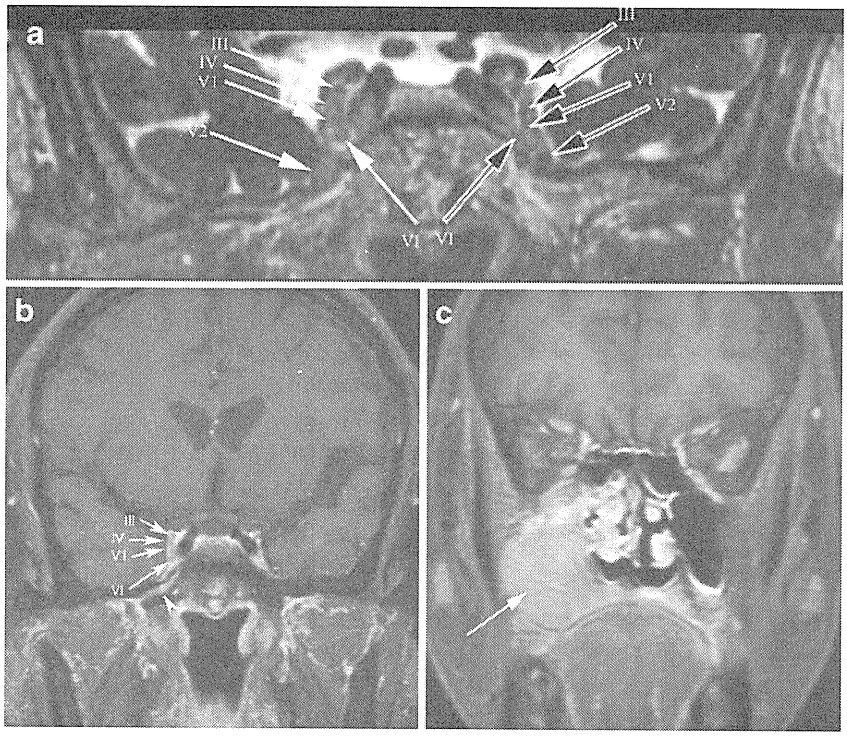

Fig. 5 Case 3 in the neoplastic group. A 64-year-old man with adenoid cystic carcinoma originating from the right maxillary sinus and invading to the right cavernous sinus who complained neuropathy of right cranial nerves (CNs) III, V_1, and VI. **a** Contrast-enhanced coronal CISS MRI (11.8/5.9) reveals right CNs III, IV, V_1, V_2, and VI (*white arrows*) with enlargement and enhancement. Left CNs III–VI appear normal (*black arrows*). **b** Contrast-enhanced coronal T1-weighted MRI with fat suppression (450/15) identify right CNs III, IV, V_1, and VI (*white arrows*) with enlargement. A band-shaped enhanced lesion is seen along the foramen ovale (*white arrowhead*), indicating the passage of tumor infiltration. **c** Contrast-enhanced coronal T1-weighted MRI with fat suppression (450/15) reveals a primary tumor of the right maxillary sinus (*white arrow*)

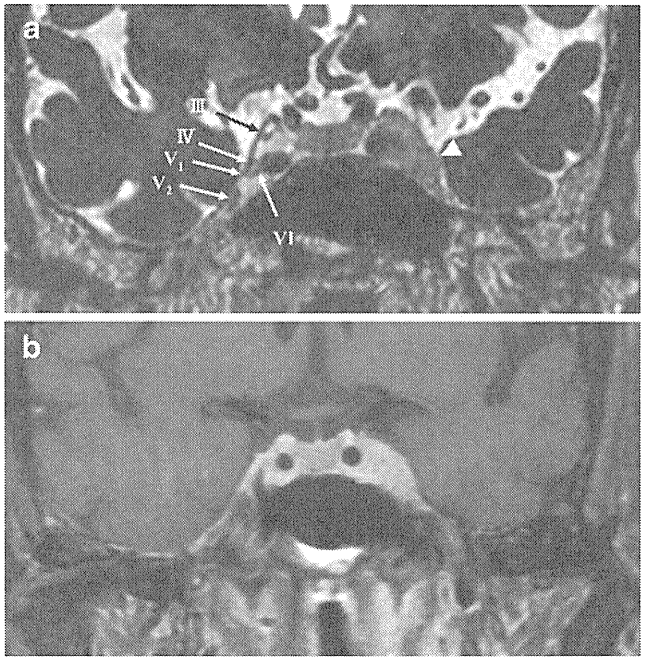

Fig. 6 Case 4 in the neoplastic group. A 76-year-old woman with papillary carcinoma with neuropathy of left cranial nerve (CN) III. **a** Contrast-enhanced coronal CISS MRI (11.8/5.9) shows the whole left cavernous is poorly enhanced and CNs are obscured (*white arrowhead*). The left cavernous sinus is enlarged. Right cavernous sinus is normally enhanced and normal CNs III, IV, V_1, V_2, and VI are detected (*arrows*). **b** Contrast-enhanced coronal T1-weighted MRI with fat suppression (450/15) reveals enlarged left cavernous sinus and lateral portion of the left cavernous sinus is slightly poorly enhanced compared to the medial portion

III, which was detected at a rate of 100% by both imaging modalities [14]. These high rates of detection could not have been obtained with the use of any other currently available methods.

The contrast-enhanced 3D CISS MRI has already been shown to be clinically useful in patients with aneurysms [18]. Hirai et al. applied this method to differentiate between paraclinoid and cavernous sinus aneurysms of the internal carotid artery. Differentiation between paraclinoid and cavernous sinus aneurysms is critical when considering treatment options. Paraclinoid carotid aneurysms pose a risk of subarachnoid hemorrhage and may therefore be considered for treatment. On the other hand, cavernous sinus aneurysms pose little or no risk of hemorrhage and are usually followed noninvasively in asymptomatic patients. The results of the Hirai et al. study showed that contrast-enhanced 3D CISS imaging yielded clear visualization of the carotid artery in the cavernous sinus and at the boundary between the CSF and cavernous sinus. They concluded that this imaging technique was helpful for distinguishing between paraclinoid and cavernous sinus aneurysms.

There are infectious as well as noninfectious types of inflammatory disease of the cavernous sinuses. Infectious diseases are usually caused by bacterial or fungal infections such as actinomycosis, rhinocerebral mucormycosis, and aspergillosis and can be complications of sinusitis [1]. Tolosa-Hunt syndrome is a well-known noninfectious inflammatory disease of the cavernous sinus. It is characterized by painful ophthalmoplegia due to nonspecific granulomatous inflammation in the cavernous sinus, superior orbital fissure, or orbital apex. Several reports have described the MR characteristics of abnormal tissue in the cavernous sinus in Tolosa-Hunt syndrome [2–11]. These characteristics include enlargement of the cavernous sinus with abnormal intensity and marked enhancement [3–8]. Haque et al. reported observing small areas of slow, gradual enhancement from the early to late phase on dynamic imaging [9]. We detected CN enlargement and enhancement in four out of five cases of Tolosa-Hunt syndrome. This is the first report of the detection of such CN abnormalities in patients with this condition (Figs. 2 and 3). Figure 4 also represented the usefulness of contrast-enhanced CISS to detect the disease involvement area as poorly enhanced findings along the superior and lateral margin of the cavernous sinus and it made obscure left CNs. Although CN itself was not detected as abnormal in this study, we can speculate that fungal infection invaded to the left cavernous sinus and caused left cranial neuropathy.

Of six neoplastic cases, nerve enlargement was observed in only one patient (case 3) with adenoid cystic carcinoma. In the other five cases, no abnormal CNs were detected because the CN itself was obscured due to the tumor mass effect or tumoral involvement (Fig. 6). Adenoid cystic carcinoma is known to exhibit infiltrative perineural spread. These pathological findings were clearly demonstrated by contrast-enhanced CISS MRI (see Fig. 5).

There are some limitations in this study. First, the detectability of cavernous sinus CNs was not 100% in the controls, with the exception of CN III. A particularly low rate of detection of CN IV was obtained [14]. Second, in many neoplastic cases, CNs were obscured and could not be identified. In those cases, it was difficult to differentiate between true pathological involvement and simply a tight attachment without pathological involvement. Third, we compared contrast-enhanced 3D CISS images to conventional 2D contrast-enhanced T1-weighted images in all but one case. The reconstructed section thickness was 0.7 mm on 3D CISS, but it was 3 mm on 2D T1-weighted images, which would cause a disadvantage to the latter method. However, the reason for the selection of 2D T1-weighted images for comparison was that almost all previous MR studies focusing on cavernous sinus disease have employed conventional contrast-enhanced 2D T1-weighted images with 3-mm thickness, and thus it is important to emphasize that contrast-enhanced 3D CISS images were superior to the previous method which was considered as a golden standard. Fourth, this study was a retrospective study; therefore, the

sequence of T1-weighted images after injection was slightly different, such as conventional 2D T1-weighted images with or without fat suppression or 3D T1-weigted images (FLASH). This study definitely showed the usefulness of contrast-enhanced 3D CISS images, but comparative T1-weighted sequences should have been unified.

Conclusions

Contrast-enhanced 3D CISS MRI provided clear images of CN abnormalities in the cavernous sinuses that have not been shown previously in vivo. This method was therefore shown to be superior to conventional contrast-enhanced T1-weighted images for the detection of abnormal CNs in both inflammatory and neoplastic conditions. We recommend contrast-enhanced 3D CISS MRI for the evaluation of diseases of the cavernous sinus.

Conflict of interest statement We declare that we have no conflict of interest.

References

1. Lee JH, Lee HK, Park JK et al (2003) Cavernous sinus syndrome: clinical features and differential diagnosis with MR imaging. AJR Am J Roentgenol 181:583–590
2. Yousem DM, Atlas SW, Grossman RI et al (1989) MR imaging of Tolosa-Hunt syndrome. AJNR Am J Neuroradiol 10:1181–1184
3. Yousem DM, Atlas SW, Grossman RI et al (1990) MR imaging of Tolosa-Hunt syndrome. AJR Am J Roentgenol 154:167–170
4. Desai SP, Carter J, Jinkins JR (1991) Contrast-enhanced MR imaging of Tolosa-Hunt syndrome: a case report. AJNR Am J Neuroradiol 12:182–183
5. Aktan S, Aykut C, Erzen C (1993) Computed tomography and magnetic resonance imaging in three patients with Tolosa-Hunt syndrome. Eur Neurol 33:393–396
6. Zournas C, Trakadas S, Kapaki E et al (1995) Gadopentetate dimeglumine-enhanced MR in the diagnosis of the Tolosa-Hunt syndrome. AJNR Am J Neuroradiol 16:942–944
7. Pascual J, Cerezal L, Canga A et al (1999) Tolosa-Hunt syndrome: focus on MRI diagnosis. Cephalalgia 19:36–38
8. de Arcaya AA, Cerezal L, Canga A et al (1999) Neuroimaging diagnosis of Tolosa-Hunt syndrome: MRI contribution. Headache 39:321–325
9. Haque TL, Miki Y, Kashii S et al (2004) Dynamic MR imaging in Tolosa-Hunt syndrome. Eur J Radiol 51:209–217
10. Cakirer S (2003) MRI findings in Tolosa-Hunt syndrome before and after systemic corticosteroid therapy. Eur J Radiol 45:83–90
11. Cakirer S (2003) MRI findings in the patients with the presumptive clinical diagnosis of Tolosa-Hunt syndrome. Eur Radiol 13:17–28
12. Casselman JW, Kuhweide R, Deimling M et al (1993) Constructive interference in steady state-3DFT MR imaging of the inner ear and rebebellopontine angle. AJNR Am J Neuroradiol 14(1):47–57
13. Shigematsu Y, Korogi Y, Hirai T et al (1999) Contrast-enhanced CISS MRI of vestibular chwanoomas: phantom and clinical studies. J Comput Assist Tomogr 23(2):224–231
14. Yagi A, Sato N, Taketomi A et al (2005) Normal cranial nerves in the cavernous sinuses: contrast-enhanced three-dimensional constructive interference in the steady state MR imaging. AJNR Am J Neuroradiol 26:946–950
15. Daniels DL, Pech P, Mark L et al (1985) Magnetic resonance imaging of the cavernous sinus. AJR Am J Roentgenol 144:1009–1014
16. Daniels DL, Czervionke LF, Bonneville JF et al (1988) MR imaging of the cavernous sinus: value of spin echo and gradient recalled echo images. AJNR Am J Neuroradiol 151 (5):1009–1014
17. Castillo M (2002) Imaging of the upper cranial nerves I, III–VIII, and the cavernous sinuses. Magn Reson Imaging Clin N Am 10:415–431
18. Hirai I, Kai Y, Morioka M et al (2008) Differentiation between paraclinoid and cavernous sinus aneurysm with contrast-enhanced 3D constructive interference in steady-state MR imaging. AJNR Am J Neuroradiol 29:130–133

MSの免疫病態のトピックス

3

冨田敦子　荒浪利昌　山村 隆
TOMITA Atsuko, ARANAMI Toshimasa, YAMAMURA Takashi/独立行政法人国立精神・神経医療研究センター免疫研究部

多発性硬化症(MS)の動物モデルではTh17細胞やTh1細胞が重要な役割を果たすが，MS病態においてはまだ一定の見解は得られていない．インターフェロンβ(IFN-β)治療抵抗性のMS患者の特徴として，IFNシグナルの亢進，血清中のIL-17FおよびIFN-βの濃度上昇が認められており，Th17偏倚が関与している可能性がある．また，MSの炎症初期病態形成には，脈絡叢から侵入したCCR6陽性Th17細胞の関与が提唱されている．抗CD20抗体であるリツキシマブの有効性から，B細胞のMS病態への関与が示され，抗体産生やT細胞からの炎症性サイトカイン産生促進を介する機序が示唆されている．

Key words
■Th17細胞
■インターフェロン(IFN)β治療抵抗性
■CCR6
■リツキシマブ
■B細胞

はじめに

多発性硬化症(MS)は，T細胞やB細胞が介在する自己免疫性脱髄性疾患である．MS患者数は年々増加し，2008年3月現在の特定疾患認定患者は1万3千人にものぼる．MS研究は，Th1/Th2バランスに立脚した病態解釈から，インターロイキン17(IL-17)を産生するTh17細胞の同定を経て新たな時代に入ったと考えられる．また，MS再発抑制の第一選択薬であるインターフェロンβ(IFN-β)に対する治療抵抗性の分子基盤，およびバイオマーカー研究においても進展がみられる．ここでは，実験的自己免疫性脳脊髄炎(EAE)やMSの病態について，Th1細胞やTh17細胞をめぐる議論を含め最近の知見を交えて概説する．

1 MSとTh1/Th17細胞

MSの原因はまだわかっていないが，髄鞘蛋白のひとつであるミエリン塩基性蛋白(myelin basic protein；MBP)のアナログ投与による症状の増悪[1]や，全身性エリテマトーデス(SLE)や1型糖尿病などの自己免疫疾患とMSに共通するMHCハプロタイプの存在[2]，EAEとMSの病態との類似から，自己免疫疾患と考えられるようになった．免疫系細胞のうち，ヘルパーT(Th)細胞は免疫反応の中心的存在であり，MSとは髄鞘蛋白反応性Th細胞が惹起する自己免疫疾患であるとされる．Th細胞の最も重要な機能のひとつが多様なサイトカイン産生であるが，Th細胞は活性化ののち，特定のサイトカイン産生細胞へと分化する(図1)．従来，自己免疫疾患においてはTh1細胞が過剰に働いており，またTh1と

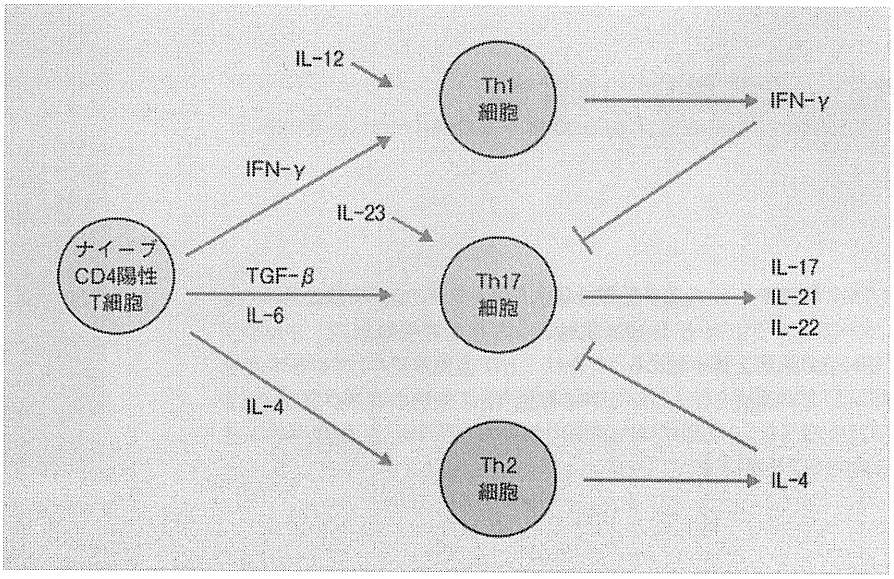

図1　CD4陽性T細胞の分化

ナイーブCD4陽性T細胞は，活性化に伴いIL-12存在下ではTh1細胞，IL-4存在下ではTh2細胞に分化する．IL-6とTGF-β存在下ではTh17細胞に分化し，IL-23はTh17細胞の増殖に働く．IFN-γとIL-4はTh17細胞の分化を抑制する．

Th2は互いに抑制的に働くことから，Th1/Th2バランスの乱れが関与すると考えられてきた．しかし近年，Th17細胞が新たなTh細胞分画として発見されてから，乾癬などの慢性炎症性疾患の病態形成に，Th17細胞が関与していることが示唆されている．同様にMSでも，これまでのTh1/Th2バランスの概念が大きく変化し，Th17細胞の病態への関与について報告されている．

MSの動物モデルであるEAEでは，Th1細胞分化に重要なIL-12の欠損マウスがEAEを発症するのに対して，Th17細胞の増殖あるいは病原性の獲得に重要なIL-23の欠損マウスではEAEが発症しないことが示されている．また，健常マウスに移入した場合，Th1細胞と比較し，Th17細胞がより重篤なEAEを惹起することも示された[3]．しかしその一方で，Th17細胞が特徴的に産生する種々のサイトカイン(IL-17A，IL-17F，IL-22など)遺伝子の欠損は，必ずしもEAE発症に影響を及ぼさないことも報告された[4]．

ヒトでは，MS髄液中でのIL-17のmRNAの増加[5]や，視神経脊髄型MS(opticospinal MS；OSMS)の髄液中IL-17蛋白濃度の増加[6]などが報告されている．また，IFN-γ，IL-17の両方のサイトカインが，炎症のプロセスに関与しているとする説もある．MS患者の髄液中では，IFN-γ産生細胞に加えてIL-17産生細胞も再発時に増加している[7]．さらには，IFN-γとIL-17を同時に産生するdouble producer細胞がより血液脳関門(blood-brain barrier；BBB)通過能が高く，MSの病巣でも多く観察される[8]ことが報告されている．しかしその一方で，IL-12とIL-23シグナルをブロックする中和抗体は，乾癬には有効であったが，MSにおいては再発抑制効果が認められなかった[9]．このような経緯から，MSにおけるTh17細胞の意義はまだ確立していない．

IFN-β responderとnon-responder

IFN-βは再発寛解型MS(relapsing-remitting MS；RRMS)の再発予防薬のひとつとして広く用いられている．IFN-βの作用機序については，炎症性サイトカインであるIFN-γの抑制，T細胞活性化の阻害，T細胞の遊走抑制，Th17細胞への分化抑制などさまざまな報告があるが，まだ一定の見解が得られていない．また，IFN-β投与により再発や活動性病巣の減少が認められるが，IFN-βに治療抵抗性のMS患者群(non-responder)も10～50％存在する．これまでnon-responderの存在は知られていたが，その分子機構およびIFN-β導入以前に両者を区別可能なバイオマーカーは不明であった．

Comabellaらは，IFN-β投与を受けたMSについて，IFN-β投与前後の末梢血液のマイクロアレイデータと2年後の治療反応性を照合し，IFN-β有効性を予測できる遺伝子を探索し

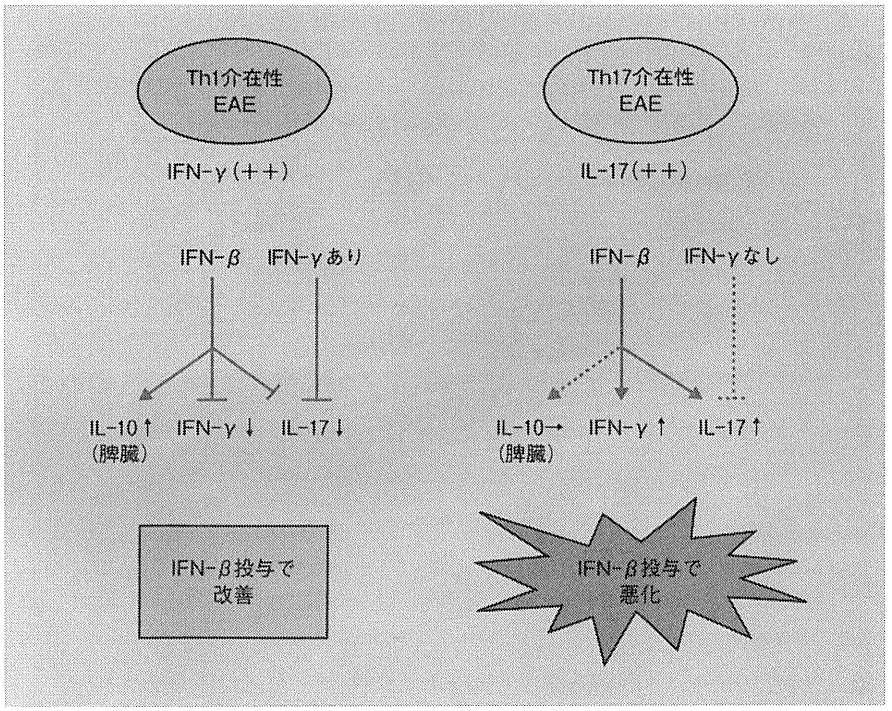

図2　サイトカインによるIFN-β反応性の違い

Th1細胞が優位な環境では，IFN-γシグナリングが存在し，IFN-β投与によるIFN-γやIL-17など炎症性サイトカインの抑制，抑制性サイトカインであるIL-10産生が起こる(左)．Th17細胞が優位な環境では，IFN-γが存在しないため，これらの反応が起こらず，症状が増悪する(右)．

た[10]．その結果，IFN-β導入後，1回以上の再発があり，かつKurtzke総合障害度スケール(EDSS)スコアが1以上増悪したnon-responderでは，薬剤投与前からtype 1 IFNシグナルに関わる遺伝子の発現が亢進していた．Non-responderの末梢血ではtype 1 IFN受容体であるIFNR1の発現が増加し，IFNR1下流の細胞内シグナル伝達分子の活性化が亢進していることが判明した．つまりnon-responderにおいては，あらかじめ内因性のIFNシグナルが亢進した状態であるために，外から加えたIFN-βによる効果が得られないとも考えられ，今後type 1 IFN関連遺伝子がIFN反応性の予測マーカーとなる可能性がある．

同時期にAxtellらはTh1細胞で誘導したEAEにはIFN-βが有効であり，逆にTh17細胞で誘導したEAEはIFN-β投与により症状の増悪がみられることを報告した[11]．Th1介在性EAEでは，IFN-β投与によりIFN-γおよびIL-17の抑制と，脾臓での抑制性サイトカインIL-10産生亢進が生じ，この効果はIFN-γノックアウトマウスでは観察されなかったことから，IFN-βが有効性を発揮するためにはIFN-γシグナルが必要と考えられた．一方，Th17介在性EAEでは，脾臓でのIL-17産生は低下するがIL-10産生に変化がなく，脊髄でIFN-γあるいはIL-17産生細胞が増加していたことから，IFN-γの存在しない環境下ではIFN-βによるIL-10産生誘導が起こらず治療効果がみられないと考えられた(図2)．さらに，MS患者のうちnon-responderでは，治療前の血清中IL-17FとIFN-β濃度がresponderに比べて高い一群が存在し，Th17に偏倚している可能性が考えられた．この一群では，あらかじめIFN-β濃度が高いためにIFN-βの治療効果が得られないのか，Th17に偏倚している状況下ではIFN-βが炎症促進に働くのか，ここでは結論が出ていない．しかし，MSの病態にはTh1に偏倚している状態とTh17に偏倚している状態が存在し，前者にはIFN-β治療が有効であるが，後者ではむしろ病態を悪化させてしまう可能性は十分ある．IFN-β投与を検討するにあたり，この点も考慮に入れる必要があると言えよう．

3 中枢神経系に至る経路

接着分子α4β1-インテグリン(VLA-4)/VCAM-1の中和抗体であるナタリズマブがMS再発抑制に有効である[12][13]ことからも，中枢神経系へのリンパ球浸潤過程を理解することは重要であるが，近年，この過程の分子機構の解析が進んでいる．中枢神経系はBBB，血液髄液関門(blood-cerebrospinal fluid barrier；BCSFB)と呼ば

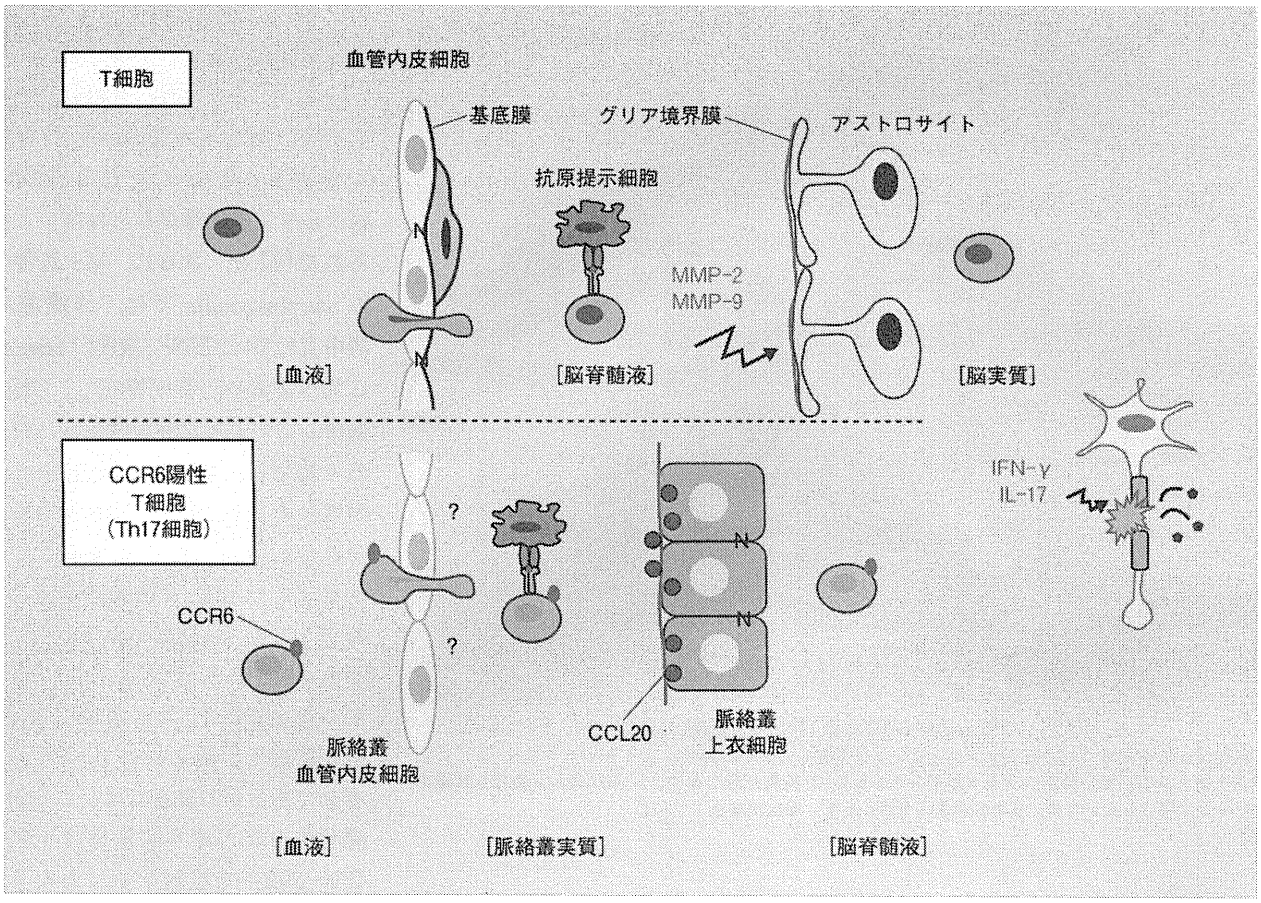

図3　中枢神経系へのリンパ球浸潤経路

上段：脳実質の血管周囲腔から浸潤する経路．活性化T細胞は，血管内皮細胞および内皮細胞基底膜を通ってくも膜下腔に至る．くも膜下腔に到達したT細胞のうち，抗原提示細胞が提示する自己抗原によって再活性化された自己反応性細胞のみが，アストロサイトの足や脳実質基底膜で構成されるグリア境界膜を通過でき，この際にmatrix metalloproteinase(MMP)と呼ばれるコラーゲン分解酵素が基底膜成分の分解に関与すると言われている．

下段：脈絡叢から浸潤する経路．T細胞が脈絡叢血管内皮細胞や上衣細胞を通過する分子メカニズムはほとんどわかっていない．脈絡叢上衣細胞はCCR6陽性T細胞(Th17細胞)のリガンドであるCCL20を豊富に発現しており，CCR6陽性T細胞の遊走に関与すると提唱されている．

れる特殊構造によって物質の移動が制限されており，炎症細胞が血管から中枢神経系に侵入するためには2つのステップが必要とされている(図3：上段)．すなわち，炎症細胞は内皮細胞内を通り抜け，髄液と交通しているperivascular spaceに入る[11]が，脳実質に侵入する際には，さらにアストロサイトの足と基底膜から構成されるグリア境界膜(glia limitans)を越える必要がある．T細胞はこの膜にはインテグリンを介して結合することができず，matrix metalloproteinase(MMP)-2，MMP-9などのMMPによって膜を変性させることで実質への侵入が可能になると推測されている．Bartholomäusらは，2光子励起顕微鏡を用いて髄膜血管表面を移動するT細胞を観察し，ミエリン抗原特異的T細胞のみならず，ovalbumin(OVA)特異的T細胞も血管内からくも膜下腔へ遊走し，活性化T細胞であれば血管外へ遊走することを示した[14]．しかし，脳実質へ浸潤したのは，ミエリン抗原特異的